PHYSICAL REVIEW B **93**, 041108(R) (2016)

Topological nematic phase in Dirac semimetals

Rui-Xing Zhang,[1] Jimmy A. Hutasoit,[2] Yan Sun,[3] Binghai Yan,[3,4] Cenke Xu,[5] and Chao-Xing Liu[1]
[1]*Department of Physics, The Pennsylvania State University, University Park, Pennsylvania 16802, USA*
[2]*Instituut-Lorentz, Universiteit Leiden, P.O. Box 9506, 2300 RA Leiden, The Netherlands*
[3]*Max Planck Institute for Chemical Physics of Solids, 01187 Dresden, Germany*
[4]*Max Planck Institute for the Physics of Complex Systems, 01187 Dresden, Germany*
[5]*Department of Physics, University of California, Santa Barbara, California 93106, USA*
(Received 7 April 2015; revised manuscript received 2 January 2016; published 26 January 2016)

We study the interaction effect in a three-dimensional Dirac semimetal and find that two competing orders, charge-density-wave orders and nematic orders, can be induced to gap the Dirac points. Applying a magnetic field can further induce an instability towards forming these ordered phases. The charge-density-wave phase is similar to that of a Weyl semimetal, while the nematic phase is unique for Dirac semimetals. Gapless zero modes are found in the vortex core formed by nematic order parameters, indicating the topological nature of nematic phases. The nematic phase can be observed experimentally using scanning tunneling microscopy.

DOI: 10.1103/PhysRevB.93.041108

Dirac semimetals are materials whose bulk valence and conduction bands touch only at certain discrete momenta, around which the low energy physics is described by gapless Dirac fermions with linear energy dispersion. The two-dimensional Dirac semimetal is realized in graphene and has been studied extensively. The three-dimensional Dirac semimetals were predicted to exist in Na_3Bi and Cd_3As_2 [1–3] and these predictions were confirmed in the recent angular resolved photon emission experiments [4,5]. The three-dimensional Dirac semimetal contains multiple copies of Weyl fermions and thus, they can exhibit nontrivial topology. Different from Weyl semimetals, the gapless nature of Dirac semimetals requires the protection of crystalline symmetries. As a consequence, by breaking some of these symmetries, Dirac semimetals can be driven towards other exotic states such as Weyl semimetals [6–10] and axionic insulators [11,12].

In this Rapid Communication, we consider the mass generation of a three-dimensional Dirac semimetal with two Dirac points protected by rotational symmetry, such as the one realized in Na_3Bi. Three different complex mass terms will arise when interaction is included in the effective Hamiltonian of a three-dimensional Dirac semimetal Na_3Bi. One complex mass is generated by charge density wave (CDW) that involves inter-Dirac-cone scattering and breaks translational symmetry. The other two complex masses come from nematic orders that break threefold rotational symmetry (C_3) by involving excitations with different spins but within a single Dirac point. Within the mean-field approximation, we map the phase diagram and find that intra-Dirac-cone interaction can spontaneously break rotational symmetry and drive the system into topological nematic phases. Electron charge distribution is identified for nematic phases, which can be directly detected by scanning tunneling microscope (STM). We further discuss localized states in topological defects as a consequence of the topological nature of nematic phases. We would like to emphasize that since gapless Dirac cones are protected by rotational symmetry, a gap opening by breaking rotation symmetry can lower the energy of a Dirac semimetal. Thus, the presence of nematic phases is generic in rotational-symmetry-protected Dirac semimetals.

Let us start by describing our model. The low energy physics of Na_3Bi is well captured by the $k\cdot p$ type of Hamiltonian density $H_0(\mathbf{k})$ around the Γ point [2]

$$H_0(\mathbf{k}) = \begin{pmatrix} M(\mathbf{k}) & Ak_+ & 0 & 0 \\ Ak_- & -M(\mathbf{k}) & 0 & 0 \\ 0 & 0 & M(\mathbf{k}) & -Ak_- \\ 0 & 0 & -Ak_+ & -M(\mathbf{k}) \end{pmatrix} \quad (1)$$

up to the second order in k, where $M(\mathbf{k}) = M_0 - M_1k_z^2 - M_2(k_x^2+k_y^2)$. The bases here are $|s,\uparrow\rangle, |p_+,\uparrow\rangle, |s,\downarrow\rangle, |p_-,\downarrow\rangle$, where for a basis $|\alpha,\sigma\rangle$, $\alpha = s, p_\pm$ is the orbital index and $\sigma = \uparrow, \downarrow$ is the spin index. The above bases are also denoted as $|\frac{1}{2}\rangle, |\frac{3}{2}\rangle, |-\frac{1}{2}\rangle, |-\frac{3}{2}\rangle$ based on the total angular momentum of each state. M_0, M_1, M_2, and A are material-dependent parameters. The part of $H_0(\mathbf{k})$ that is proportional to the identity is not important and has been neglected. The energy dispersion is $E(\mathbf{k}) = \pm\sqrt{M^2(\mathbf{k}) + A^2k_+k_-}$ and two gapless points are located at $K_i = (0,0,(-1)^i\sqrt{M_0/M_1})$, with $i \in \{1,2\}$. The low energy effective Hamiltonian around K_1 and K_2 can be expanded from (1), and it is given by $\hat{H}_0 = \sum_{\mathbf{k}} \Psi^\dagger(k)\tilde{H}_0\Psi(k)$ in the second quantized language, where

$$\begin{aligned} \Psi(k) = (&c_{k,1,s,\uparrow}, c_{k,1,p,\uparrow}, c_{k,1,s,\downarrow}, c_{k,1,p,\downarrow}, \\ &c_{k,2,s,\uparrow}, c_{k,2,p,\uparrow}, c_{k,2,s,\downarrow}, c_{k,2,p,\downarrow})^T, \\ \tilde{H}_0 = &Ak_x\alpha_0\otimes\Gamma_3 - Ak_y\alpha_0\otimes\Gamma_4 + m(k_z)\alpha_3\otimes\Gamma_5, \end{aligned} \quad (2)$$

$\mathbf{k} = (k_x,k_y,k_z)$ is the momentum relative to the Dirac points K_i, $m(k_z) = -2\sqrt{M_0M_1}k_z$, and $c^\dagger_{k,i,a,\sigma}$ creates an electron with a orbital and spin σ at $K_i + k$. We also denote $c_{k,i,p_\pm,\sigma}$ as $c_{k,i,p,\sigma}$ for brevity. $\vec{\sigma},\vec{\tau},\vec{\alpha}$ are Pauli matrices characterizing spin, orbital, and valley degrees of freedom. Γ matrices are defined as $\Gamma_{1,2,3} = \sigma_{1,2,3}\otimes\tau_1$, $\Gamma_4 = \sigma_0\otimes\tau_2$, and $\Gamma_5 = \sigma_0\otimes\tau_3$. It is easy to see that they obey Clifford algebra $\{\Gamma_i,\Gamma_j\} = 2\delta_{i,j}$.

We note that $\hat{H}_0$ is the minimal model for Dirac semimetals with time-reversal (TR) symmetry and inversion symmetry. To describe the effective Dirac behavior of electrons near K_i, we keep only the linear terms in k. It should be emphasized that including other higher order off-diagonal terms cannot

open a gap at K_1 and K_2 since two degenerate states transform differently under threefold rotational symmetry.

The fermionic field operator Ψ can be thought of as four copies of Weyl fermions: two with left-handed chiralities and the other two right-handed. Here, we focus on the case with charge conservation and thus, the mass terms can only be formed by interactions of two Weyl fermions with opposite chiralities and therefore, there are two possible mass terms. The first one comes from two Weyl fermions with opposite chiralities at different momenta (K_1 and K_2). This term breaks translational symmetry and corresponds to CDWs. Such a term can also be found in Weyl semimetals and is responsible for axion insulator phases [11–13]. Since Dirac semimetals can be viewed as two copies of Weyl semimetals that conserve TR symmetry, the gapped phase due to CDWs should also be thought of as two copies of axion insulator phases which are related to each other by TR symmetry. The second mass term couples two Weyl fermions at the same momentum (K_1 or K_2). Since the gapless nature of Dirac semimetals at a fixed momentum is protected by C_3 symmetry, it is natural to expect this mass term to break rotation symmetry but preserves translational symmetry. This corresponds to a nematic phase. Therefore, these mass terms should be generated by the following order parameters:

$$\text{CDW: } D_{\alpha,\beta,\sigma} = \langle c^{\dagger}_{k,1,\alpha,\sigma} c_{k,2,\beta,\sigma} \rangle,$$
$$\text{nematic: } N_{\alpha,\beta,K_i} = \langle c^{\dagger}_{k,i,\alpha,\uparrow} c_{k,i,\beta,\downarrow} \rangle. \quad (3)$$

On the other hand, possible mass terms should then anticommute with $\tilde{H}_0$ and there are only six of such terms: $\alpha_0 \otimes \Gamma_1$, $\alpha_0 \otimes \Gamma_2$, $\alpha_1 \otimes \Gamma_5$, $\alpha_2 \otimes \Gamma_5$, $\alpha_3 \otimes \Gamma_1$, $\alpha_3 \otimes \Gamma_2$. Based on the above analysis, we identify all possible mass terms and introduce

$$N^*_{s,p,1} = N^*_{p,s,1} = \Delta_1 + \Delta_2,$$
$$N^*_{s,p,2} = N^*_{p,s,2} = \Delta_1 - \Delta_2,$$
$$D^*_{s,s,\uparrow} = D^*_{s,s,\downarrow} = -D^*_{p,p,\uparrow} = -D^*_{p,p,\downarrow} = \Delta_3, \quad (4)$$

where Δ_j's are generally complex: $\Delta_j = |\Delta_j| e^{i\theta_j}$ ($j \in 1,2,3$).

To dynamically generate these mass terms, we consider an effective interaction between different species of Dirac fermions as given by

$$\hat{H}_{int} = U \sum_k \sum_i \rho_i(k)\rho_i(k) + V \sum_k \sum_{i \neq j} \rho_i(k)\rho_j(k), \quad (5)$$

where $\rho_i = \sum_{\alpha,\sigma} c^{\dagger}_{k,i,\alpha,\sigma} c_{k,i,\alpha,\sigma}$ are the density operators. Here, the U term describes the interaction between two electrons near one momentum K_i while V term describes that of electrons between K_1 and K_2. This effective interaction can be obtained from the Coulomb interaction, as shown in the Supplemental Material [14].

The full Hamiltonian can then be treated within the mean-field approximation (see the Supplemental Material [14] for details); the free energy at zero temperature is then given by

$$F = H_{MF} - \sum_{E_k \in \text{occupied}} E_k(|\Delta_1|,|\Delta_2|,|\Delta_3|,\theta). \quad (6)$$

Here E_k is the excitation spectrum in the mean-field level, whose detailed expression is shown in the Supplemental Material [14]. $\theta = \theta_1 - \theta_2$ represents the phase difference between the two nematic order parameters. To minimize the free energy, a state where $\theta = \frac{\pi}{2}$ is favored. We establish self-consistency equations to map the phase diagram in Fig. 1(a). The semimetallic phase is relatively stable under weak interaction because the density of states vanishes at Dirac points. As the interaction strength exceeds critical value U_c (V_c), the system develops a gap. In the large U (V) limit, the system favors nematic (CDW) ordering. Starting from the bicritical point (U_c, V_c), the system will go across a first-order phase transition at the $U = V$ line between the CDW and nematic phases.

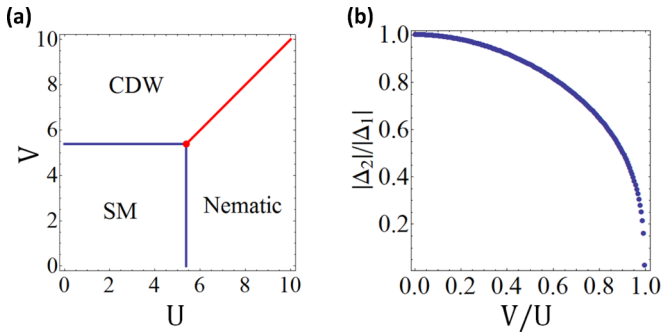

FIG. 1. (a) Phase diagram of interacting 3D Dirac semimetal Na_3Bi. (b) In the nematic phase, the ratio between Δ_2 and Δ_1 is plotted as a function of V/U.

The ordered phase of CDW is similar to that in Weyl semimetals, the physical consequence of which has been discussed in detail in [11–13]. For our system, the CDW is along the k_z direction with the wave vector $\mathbf{Q} = 2\sqrt{M_0/M_1}\hat{z}$, which can be in principle observed in an STM. Chiral modes have been proposed to exist at the dislocation line of Weyl semimetals, but since our TR invariant system is a copy of two Weyl semimetals, we have two copies of chiral modes that are TR partners and thus, our system exhibits helical modes.

What is really unique in the Dirac semimetals is the nematic phase. This nematic phase is actually a superposition of two inequivalent nematic orders Δ_1 and Δ_2 with a phase difference of $\frac{\pi}{2}$. By applying TR operation $\Theta = \alpha_1 \otimes i\sigma_2 \otimes \tau_0$, we find Δ_1 breaks TR symmetry, while Δ_2 preserves TR symmetry. In Fig. 1(b), the coexistence of two nematic orders is numerically confirmed. As the ratio V/U increases from 0 to 1, we find that the ratio Δ_2/Δ_1 decreases from 1 to 0. This indicates that the system spontaneously breaks TR symmetry in the nematic phase. Next, we will discuss several physical phenomena of nematic phases, which can be observed in experiments.

The first observable is the charge distribution. Since the mass term of nematic orders couples $|\pm\frac{3}{2}\rangle$ to $|\pm\frac{1}{2}\rangle$, we expect the charge distribution in one unit-cell breaking threefold rotation. Since the charge distribution cannot be extracted from the effective Hamiltonian, we consider a more realistic $k \cdot p$ Hamiltonian based on the first-principles calculations. The method has been successfully applied to the construction of the effective Hamiltonian of topological insulator materials [15], and we only describe our procedure briefly here. The eigenwave functions at $k = 0$ can be expanded in terms of plane waves in the first-principles calculations. Here, 36 bands are taken into account, denoted as $|n\rangle$ ($n = 1,2,\ldots,36$). We

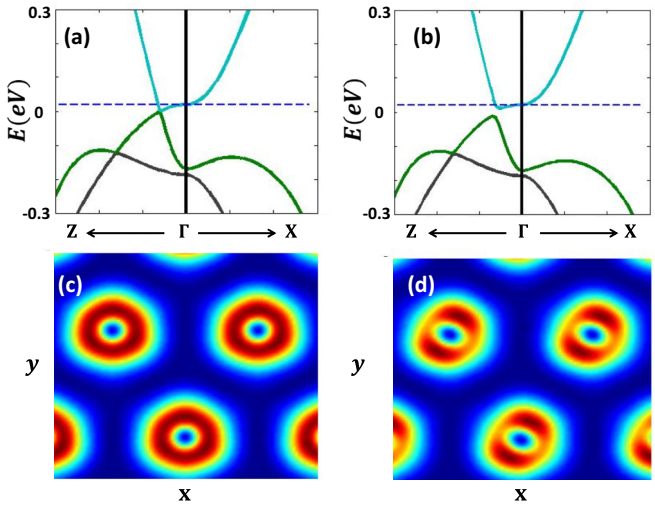

FIG. 2. The energy dispersion from realistic $k \cdot p$ theory and LDOS for one Bi layer. (a) and (c) are for free semimetals, while (b) and (d) are for the interacting case. In the LDOS plot, red (blue) represents a large (small) LDOS.

act the crystal Hamiltonian with periodic potential on the basis and obtain the $k \cdot p$ Hamiltonian $H^{kp}_{nm} = (E_n + \frac{\hbar^2 k^2}{2m})\delta_{nm} + \frac{\hbar}{m} k \cdot p_{nm}$, where E_n is the eigenenergy for the n band at $k = 0$, m is electron mass, and $p_{nm} = \langle n|p|m\rangle$ is the matrix element. We diagonalize this 36×36 Hamiltonian and the energy dispersion is shown in Fig. 2(a), which qualitatively fits to that from the first-principles calculations. In particular, a level crossing between conduction and valence bands, which corresponds to Dirac points, can be seen along the Γ-Z line. From the eigenwave functions, one can show that the conduction and valence bands indeed belong to the $|\pm\frac{3}{2}\rangle$ and $|\pm\frac{1}{2}\rangle$ states, respectively. Thus, these two states cannot be coupled to each other along the Γ-Z line. As discussed above, the interaction can introduce the coupling between these two states in the nematic phase. Therefore, we can add a constant coupling between the $|\pm\frac{1}{2}\rangle$ and $|\mp\frac{3}{2}\rangle$ states near the Fermi energy in our $k \cdot p$ Hamiltonian, leading to a gap opening, as shown in Fig. 2(b). To show that the obtained states possess nematic orders, we calculate the local density of states (LDOS) in the x-y plane for the Bi layer. As shown in Fig. 2(c), without interaction, the maxima of the LDOS (red) appear as an isotropic ring around the position of Bi atoms, corresponding to the $p_\pm$ orbitals of Bi atoms. The spatial distribution of LDOS respects threefold rotation symmetry. After adding the coupling term between the $\pm|\frac{1}{2}\rangle$ and $\mp|\frac{3}{2}\rangle$ states, the isotropic ring evolves into two peaks pointing in a certain direction, thus breaking C_3 rotation [see Fig. 2(d)]. This corresponds exactly to the nematic phase. Such electron density distribution can be directly measured through scanning tunneling microscopy.

The second phenomenon is the appearance of gapless modes in topological defects of the nematic phase, revealing the topological nature of this phase. Complex mass terms $\Delta = |\Delta|e^{i\theta}$ in a Dirac system are highly nontrivial in the sense that their phases θ are identified as dynamical axion fields, which will give rise to bulk axionic terms in the form of $\theta\epsilon^{\mu\nu\rho\sigma}F_{\mu\nu}F_{\rho\sigma}$ [11,12,16–21]. In two-dimensional (2D) Dirac systems, complex mass terms will show up as a $U(1)$ or $\mathbb{Z}_n$ vortex structure in both graphene [22,23] and π-flux square lattice [24,25] in the presence of interactions. As a consequence, zero modes will localize at the vortex centers carrying fractionalized charges. In three-dimensional (3D) Weyl/Dirac systems, those zero modes extend to one-dimensional chiral modes that go through the center of the vortices along the z direction [11,12]. These are known as axion strings. As is in the case of CDW, we expect a similar physics to occur in the vortex of nematic order parameters.

By applying in-plane vortex structures for the complex nematic order parameters, our system at fixed k_z can be directly mapped into previous 2D Dirac systems. Therefore, zero modes are expected to show up at both K_1 and K_2. To verify this, a numerical calculation is performed in a layered 2D vortex configuration. We keep the periodicity in the z direction, while placing open boundary conditions in the x-y plane. For simplicity, on a 32×32 square lattice, we place a $U(1)$ vortex-antivortex pair structure instead of the actual $\mathbb{Z}_3$ vortices. We visualize these vortex structures in Fig. 3(b) by the arrow indicating phase information of following site-dependent order parameters [24]:

$$\tilde{\Delta}_1(x,y,k_z) = |\Delta_1|\frac{(\omega-\omega_1)(\omega-\omega_2)^*}{|(\omega-\omega_1)(\omega-\omega_2)|},$$
$$\tilde{\Delta}_2(x,y,k_z) = k_z\frac{|\Delta_2|}{|\Delta_1|}\tilde{\Delta}_1(x,y,k_z). \quad (7)$$

Here, $\omega = x + iy$ is a complex coordinate and $\omega_j = x_j + iy_j$ is the complex coordinate of vortex ($j = 1$) or antivortex ($j = 2$) center. As shown in Fig. 3(a), the bulk dispersion is gapped, while gapless modes penetrate the bulk gap twice at two different momenta. In Fig. 3(b), we plot the LDOS at $E_F = 0$ together with vortex configurations in real space. It is confirmed that these modes are highly localized at the vortex (antivortex) center. The gapless nature of these modes relies on the fact that they are separated at different momenta, and requires the translational symmetry along the z direction.

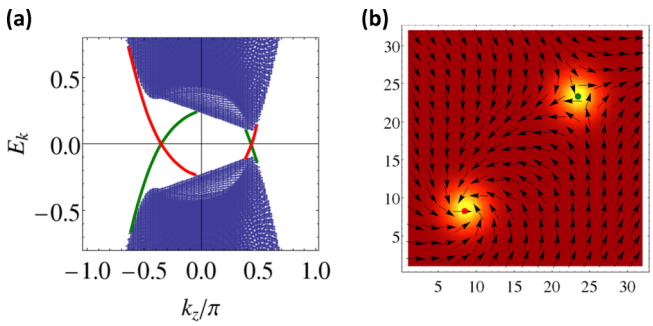

FIG. 3. (a) The fermionic spectrum in a $U(1)$ vortex-antivortex configuration on a 32×32 square lattice with open boundary conditions. We choose the following set of parameters: $M_0 = -0.6$, $M_1 = -0.3$, $M_2 = -0.4$, $A = 0.4$, $|U||\Delta_1| = 0.25, |U||\Delta_2| = 0.1$. Gapless energy bands in red (green) are localized at the vortex (antivortex) center. (b) LDOS at $E_F = 0$ is plotted which clearly shows zero modes are localized at vortex or antivortex center. The red (green) dot shows the location of a vortex (antivortex) center, while yellow (red) represents a large (small) LDOS.

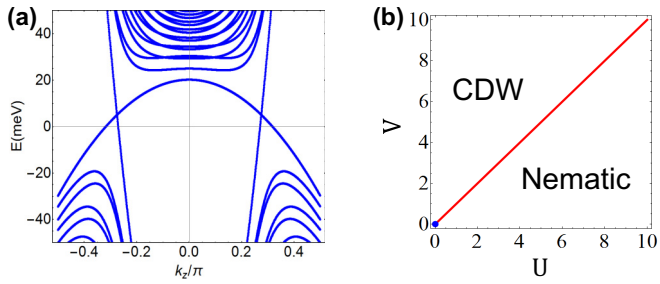

FIG. 4. (a) Landau level dispersion along k_z with magnetic field $B = 10$ T. (b) Phase diagram of Na_3Bi under magnetic field and interaction.

So far, we have discussed the effects of interaction in driving Dirac semimetals towards other phases. However, those phases along with their novel physical phenomena can only be realized under relatively strong interaction. To overcome this difficulty, one can apply a magnetic field along the z direction such that Landau levels emerge. Similar strategies have been applied to achieve quantum Hall ferromagnetism in graphene systems [26,27], where spin-orbital coupling (SOC) is almost absent. The strong SOC in Dirac semimetals, however, tends to tilt spins. As a result, CDW and nematic phases are more likely to be favored than ferromagnetism in Dirac semimetals. The Landau levels in Dirac semimetals have been observed experimentally [28–31]. Even though the higher Landau levels of Na_3Bi are gapped, the lowest Landau levels (LLLs) are gapless at K_i $(i = 1,2)$ (see Fig. 4). We identify this degeneracy to be a crossing between $|s,\uparrow\rangle$ and $|p,\downarrow\rangle$ states, which is protected from developing a gap by C_3 symmetry along the (001) axis. To describe the low energy physics of the gapless LLLs, we define a four-component spinor, $\Psi^\dagger = (c^\dagger_{k,1,s,\uparrow}, c^\dagger_{k,1,p,\downarrow}, c^\dagger_{k,2,s,\uparrow}, c^\dagger_{k,2,p,\downarrow})$. Mass terms in Eq. (4) are reduced to (1) density wave: $D_1 = D_{s,s,\uparrow}$, $D_2 = D_{p,p,\downarrow}$; (2) nematic: $N_1 = N_{s,p,K_1}$, $N_2 = N_{s,p,K_2}$. Through a similar mean-field analysis (see the Supplemental Material), the free energy at zero temperature is given by $F = H_{MF} - \sum_i \sum_{k_z} \sqrt{m(k_z)^2 + \xi_i}$ where $m(k_z) = -2\sqrt{M_1(M_0 - \frac{M_2}{l^2})}k_z$. $\xi_{1,2}$ are functions of order parameters $D_{1,2}$ and $N_{1,2}$, whose detailed expressions are explicitly shown in the Supplemental Material [14].

By minimizing the free energy, we obtain the phase diagram as shown in Fig. 4(b). Instability happens for arbitrarily weak repulsive interaction [12,13] and as one tunes the interaction to go across $V/U = 1$, the system undergoes a phase transition from a CDW phase to a nematic phase or vice versa. Let us focus on the nematic regime $(D_{1,2} = 0)$ and the corresponding self-consistent equations can be solved analytically. As is shown in the Supplemental Material [14], the critical temperature that characterizes a phase transition from semimetallic phase to the nematic phase is

$$T_c = \frac{2e^\gamma v_f \Lambda}{\pi k_B} e^{-(v_f \Lambda/U)(h/eBS)}, \tag{8}$$

where Λ is the momentum cutoff and $v_f = |\frac{m(k_z)}{k_z}|$ is the Fermi velocity. $\gamma = 0.577\ldots$ is the Euler constant and k_B is the Boltzmann constant. We have considered a sample with a finite area S in the x-y plane. When $T < T_c$, nonzero nematic ordering will always be formed for arbitrary U. In the zero-temperature limit, the magnitude of order parameter can be solved [14,32]: $|N_1| \approx \frac{2v_f\Lambda}{U} e^{\frac{-2\pi v_f \Lambda}{U}\frac{h}{eBS}}$. This expression indicates that a larger energy gap will show up for a larger magnetic field. This instability under magnetic fields is a direct result of the finite Landau level degeneracy. This suggests the necessary condition for the instability is that the cyclotron length is much smaller than the sample size. In the Supplemental Material [14], we further discuss the existing experiments studying LLs of Dirac semimetals, and predict possible evidence of nematic phases in STM measurements of Landau levels.

We acknowledge the helpful discussion with X. L. Qi. C.-X.L. acknowledges the support from Office of Naval Research (Grant No. N00014-15-1-2675) and from the Penn State MRSEC, Center for Nanoscale Science, under the Award NSF DMR-1420620. J.H. is supported by NSF Grants No. DMR-1005536 and No. DMR-0820404 (Penn State MRSEC) during the early part of this work, and later by the Netherlands Organization for Scientific Research (NWO/OCW) through the D-ITP consortium. C.X. is supported by the the David and Lucile Packard Foundation and NSF Grant No. DMR-1151208.

[1] S. M. Young, S. Zaheer, J. C. Y. Teo, C. L. Kane, E. J. Mele, and A. M. Rappe, Phys. Rev. Lett. **108**, 140405 (2012).
[2] Z. Wang, Y. Sun, X.-Q. Chen, C. Franchini, G. Xu, H. Weng, X. Dai, and Z. Fang, Phys. Rev. B **85**, 195320 (2012).
[3] Z. Wang, H. Weng, Q. Wu, X. Dai, and Z. Fang, Phys. Rev. B **88**, 125427 (2013).
[4] Z. Liu, B. Zhou, Y. Zhang, Z. Wang, H. Weng, D. Prabhakaran, S.-K. Mo, Z. Shen, Z. Fang, X. Dai *et al.*, Science **343**, 864 (2014).
[5] Z. K. Liu, J. Jiang, B. Zhou, Z. J. Wang, Y. Zhang, H. M. Weng, D. Prabhakaran, S. K. Mo, H. Peng, P. Dudin *et al.*, Nat. Mater. **13**, 677 (2014).
[6] A. A. Burkov and L. Balents, Phys. Rev. Lett. **107**, 127205 (2011).
[7] G. B. Halász and L. Balents, Phys. Rev. B **85**, 035103 (2012).
[8] C. Zhang, S.-Y. Xu, I. Belopolski, Z. Yuan, Z. Lin, B. Tong, N. Alidoust, C.-C. Lee, S.-M. Huang, H. Lin *et al.*, arXiv:1503.02630.
[9] B. Q. Lv, H. M. Weng, B. B. Fu, X. P. Wang, H. Miao, J. Ma, P. Richard, X. C. Huang, L. X. Zhao, G. F. Chen *et al.*, Phys. Rev. X **5**, 031013 (2015).
[10] S.-Y. Xu, I. Belopolski, N. Alidoust, M. Neupane, C. Zhang, R. Sankar, S.-M. Huang, C.-C. Lee, G. Chang, B. Wang *et al.*, Science **349**, 613 (2015).
[11] Z. Wang and S.-C. Zhang, Phys. Rev. B **87**, 161107 (2013).
[12] B. Roy and J. D. Sau, Phys. Rev. B **92**, 125141 (2015).
[13] K.-Y. Yang, Y.-M. Lu, and Y. Ran, Phys. Rev. B **84**, 075129 (2011).

[14] See Supplemental Material at http://link.aps.org/supplemental/10.1103/PhysRevB.93.041108 for details.
[15] C.-X. Liu, X.-L. Qi, H. J. Zhang, X. Dai, Z. Fang, and S.-C. Zhang, Phys. Rev. B **82**, 045122 (2010).
[16] A. A. Zyuzin and A. A. Burkov, Phys. Rev. B **86**, 115133 (2012).
[17] R. D. Peccei and H. R. Quinn, Phys. Rev. Lett. **38**, 1440 (1977).
[18] F. Wilczek, Phys. Rev. Lett. **40**, 279 (1978).
[19] S. Weinberg, Phys. Rev. Lett. **40**, 223 (1978).
[20] F. Wilczek, Phys. Rev. Lett. **58**, 1799 (1987).
[21] R. Li, J. Wang, X.-L. Qi, and S.-C. Zhang, Nat. Phys. **6**, 284 (2010).
[22] C.-Y. Hou, C. Chamon, and C. Mudry, Phys. Rev. Lett. **98**, 186809 (2007).
[23] C. Chamon, C.-Y. Hou, R. Jackiw, C. Mudry, S.-Y. Pi, and G. Semenoff, Phys. Rev. B **77**, 235431 (2008).
[24] B. Seradjeh, C. Weeks, and M. Franz, Phys. Rev. B **77**, 033104 (2008).
[25] C. Weeks and M. Franz, Phys. Rev. B **81**, 085105 (2010).
[26] K. Nomura and A. H. MacDonald, Phys. Rev. Lett. **96**, 256602 (2006).
[27] A. F. Young, C. R. Dean, L. Wang, H. Ren, P. Cadden-Zimansky, K. Watanabe, T. Taniguchi, J. Hone, K. L. Shepard, and P. Kim, Nat. Phys. **8**, 550 (2012).
[28] S. Jeon, B. B. Zhou, A. Gyenis, B. E. Feldman, I. Kimchi, A. C. Potter, Q. D. Gibson, R. J. Cava, A. Vishwanath, and A. Yazdani, Nat. Mater. **13**, 851 (2014).
[29] L. P. He, X. C. Hong, J. K. Dong, J. Pan, Z. Zhang, J. Zhang, and S. Y. Li, Phys. Rev. Lett. **113**, 246402 (2014).
[30] Y. Zhao, H. Liu, C. Zhang, H. Wang, J. Wang, Z. Lin, Y. Xing, H. Lu, J. Liu, Y. Wang *et al.*, Phys. Rev. X **5**, 031037 (2015).
[31] S. K. Kushwaha, J. W. Krizan, B. E. Feldman, A. Gyenis, M. T. Randeria, J. Xiong, S.-Y. Xu, N. Alidoust, I. Belopolski, T. Liang *et al.*, APL Mater. **3**, 041504 (2015).
[32] R. Shankar, Rev. Mod. Phys. **66**, 129 (1994).